2

High-Pressure Carbonaceous Phases as Minerals

Oliver Tschauner

ABSTRACT

High-pressure carbonaceous minerals establish a link between one of the most abundant chemical elements and processes that occur at high pressures, either in the interior of the Earth or during shock-metamorphosis in space or on Earth. Diamonds from the Earth's mantle carry inclusions of carbides, carbonates, methane, and carbon-dioxide. These inclusions elucidate diamond formation and the carbon recycling in the mantle. This chapter focuses on these inclusion minerals themselves, the means of detection, and the reconstruction of pressure-temperature conditions of their formation in the mantle.

2.1. INTRODUCTION

Understanding the evolution of the interior of Earth requires correlation of geochemical and geophysical data. However, geochemistry and geophysics probe different time spans and, probably, also different spatial scales of reservoirs (Helffrich & Wood, 2001; van Keken et al., 2002): The differentiation of chemical elements in Earth often occurs on timescales that are beyond the survival of distinguishable seismic features of the geophysical heterogeneities that have caused them, such as a particular subducted slab or mantle plume. In addition, noticeable geochemical reservoirs in the mantle may not even correspond to a particular zone or region in Earth which can be detected through seismic waves but are finely dispersed in the mantle or simply reflect a temporal evolution of isotopic signatures. Correlation becomes the more difficult the deeper parts of the mantle shift into scope: In absence of large bodies of rocks obducted from great depth, individual grains of minerals that were entrapped in diamonds are the only direct witnesses of processes in the deeper Earth, and the mineralogical and chemical information obtained from them has to provide the constraints on geochemical deep-mantle signatures and their correlation with seismic features and with geodynamic models. Minerals that originate from sublithospheric mantle may have transformed back to phases more stable at shallower depth but may still carry the chemical signatures of their origin because diamond is a chemically inert host material of exceptionally high confining pressures and temperatures (Brenker et al., 2002; Harte et al., 1999; Shirey et al., 2013; D. Smith et al., 2018; Sobolev, 1997; Stachel et al., 2000; Walter et al., 2011). In rare cases, diamonds conserve high-pressure minerals in their original structure by supporting high residual pressures of these inclusions that prevent transformation to lower-pressure polymorphs (Howell et al., 2012; Navon, 1991; Nestola et al., 2018; Pearson et al., 2014; Tschauner et al., 2018). The residual pressure of these inclusions corresponds to the end point of a thermodynamic path that connects current residual pressure at 300 K with the pressure and temperature of entrapment of this inclusion. Because of the high plastic yield limit, low compressibility, and low thermal expansivity of diamond, these paths are nearly isochoric (Navon, 1991, 2017; Tschauner et al., 2018), although thermoelastic corrections for diamond have to be made or the approach of a corrected isochore is substituted by the use of isomekes (Angel et al., 2014; Nasdala et al., 2003). This overall simple, monotonic path makes the reconstruction of the conditions of entrapment of these inclusions comparatively much easier than in case of inclusions in other minerals. For the same reason, inclusions in diamond differ from inclusions in garnets or other minerals, which have much lower plastic deformation limits than diamond by supporting inclusions with

Department of Geoscience, University of Nevada–Las Vegas, Las Vegas, Nevada, USA

Carbon in Earth's Interior, Geophysical Monograph 249, First Edition. Edited by Craig E. Manning, Jung-Fu Lin, and Wendy L. Mao.

residual pressures in the range of several GPa. Exhumation speed may be estimated from isotope-data of inclusions whose pressure has been determined in prior geochemical analysis or from the nitrogen-aggregation state of the host diamond (Taylor et al., 1990). Both methods come with challenges: Inclusions with high residual pressure appear to be generally small (micrometer-scale) because larger inclusions cause accordingly higher local stresses in the surrounding diamond and result in cracking and annealing at shallow depth. However, isotope analysis of very small inclusions is very difficult. The analysis of nitrogen aggregation states is in principle straightforward. However, many diamonds are not homogeneous containing zones of different nitrogen concentration and aggregation. Overall, the assessment of exhumation speed is less straightforward than the assessment of pressure and temperature of the source region.

As it will be shown, high-pressure carbonaceous phases play an important role in assessing the global carbon cycle; they are conserved within and connected to the formation of diamonds, and they place diamond formation into the context of the global carbon cycle.

2.1.1. High-Pressure Minerals in Meteorites and Impactites

High-pressure minerals also occur (and are actually found more frequently than in diamonds) in a very different environment: Meteorites and terrestrial crustal rocks that have been subjected to severe shock-metamorphism during asteroid impacts (Sharp & DeCarli, 2006; Stöffler et al., 1991) contain veins and pockets of minerals that otherwise only occur in the deep mantle of rocky planets like Earth. A comprehensive list of meteorite minerals, including shock-metamorphic minerals, can be found in Rubin and Ma (2017). A list of the more recently discovered high-pressure minerals is given by Ma (2018). Carbon and carbonaceous species are abundant in the solar system, and the occurrence of diamond in carbonaceous chondrites is established (Anders & Zinner, 1993). Moissanite (SiC-2H) (Anders & Zinner, 1993) and other carbides have been found as well in iron-meteorites, ureilites, enstatite-chondrites, achondrites, and in CAIs (calcium-aluminum rich inclusions that formed under highly reducing conditions early in the solar system). Most of these minerals have not formed at high pressure, and the reader is referred to the recent comprehensive account of meteorite minerals by Rubin and Ma (2017). Besides diamond, lonsdaleite (the 2H polytype of diamond) has been reported but was recently discredited (Nemeth et al., 2014). Furthermore, chaoite and other structurally uncharacterized dense forms of carbon were reported from terrestrial impact craters (El Goresy & Donnay, 1968; El Goresy et al., 2003). At the high pressures and temperatures in the isobaric core of large impacts carbonates dissociate (Schulte et al., 2009), whereas the decaying shockwave in the more remote regions of the bedrock is not known to cause irreversible transformations of carbonates to high-pressure forms. Thus, with diamond as the only well-characterized impact-generated high-pressure phase of a carbonaceous species (Anders & Zinner, 1993; Hough et al., 1995), we do not further discuss shock-related dense carbonaceous phases here. Novel micrometer and submicrometer structural and spectroscopic probes may reveal more impact-related carbonaceous phases in the future. Occurrence and formation of diamonds from impacts, meteorites, and interplanetary and interstellar dust are interesting topics by themselves but more fit for a monograph about diamond rather than carbon in general.

Within the context of this monograph about carbon in natural systems we dedicate this chapter to two particular types of terrestrial occurrences of carbonaceous minerals: (a) naturally occurring dense polymorphs of C-rich phases that are stable or that form at high pressure and (b) occurrences of carbonaceous minerals that retain high residual pressures as inclusions in diamond.

We use the term *carbonaceous* in reference to phases with carbon as constituting element. We discuss a few cases where carbon as minor component in a solid high-pressure phase induces a characteristic change in structure. This chapter is about high-pressure carbonaceous minerals. Minerals are crystalline phases by definition (Nickel & Grice, 1998); hence, state and properties of dense liquid or fluid carbonaceous phases are beyond our scope.

We follow the conventional classification scheme of minerals by chemical classes starting with elemental minerals, alloys, and carbides, and progressing to sulfides, oxides, and so on (Dana, 1869). While this scheme has become problematic because it largely ignores structural relations between minerals of different composition and fundamental differences in chemical bonds of phases of same composition, it causes no significant issues in discussing a topic that is already restricted by its focus on carbon as constituent atomic species and may serve here as a known and accepted framework. Consequently, the number of subchapters is limited to elements, carbides, oxides, and carbonates. Unless stated otherwise, we henceforth reserve the term *diamond* here to natural terrestrial diamonds that are not impact related.

2.2. CARBONACEOUS PHASES AS INCLUSION IN DIAMOND: ELEMENTS AND CARBIDES

2.2.1. Diamond in Diamond: Indication for Methane Breakdown in the Lithospheric Mantle

The first carbonaceous phase that occurs as inclusion in diamonds is, seemingly paradoxically, diamond. Terrestrial diamonds are composed of single crystal

domains on the scale of tens of micrometers to millimimeters or more. Mosaicity of diamonds varies extensively (see, for instance, Shirey et al., 2013), and many diamonds exhibit zones or kernels of different age, orientation, and domain sizes (Boyd et al., 1994; Shirey et al., 2013). In addition, domains of very fine-grained diamond are found within single crystal diamonds. Polycrystalline diamond is found in the surrounding of inclusions of other minerals, at the surface of single crystal diamonds, and other locations where mechanical damage disrupted the original large-scale crystalline order. A distinct occurrence of polycrystalline diamond is very fine-grained, isolated, polycrystalline diamond inclusions within diamond single crystals. These inclusions are fully encapsulated in well-crystallized single crystal domains of low strain. The grain size ranges from 10 nm to ¼ μ m based on the Scherrer equation that correlates noninstrumental powder diffraction peak width with average grain size. The spatial extension of these inclusions ranges from a few to a few tens of micrometers. To our knowledge, the pressure of these fine polycrystalline diamond inclusions is always ambient to nearly ambient and not different from that of the surrounding single crystal diamond host lattice beyond uncertainty. An example of polycrystalline diamond in single crystal diamond is given in Figure 1.1. It is indicative that these pockets of fine-grained polycrystalline diamond are a result of breakdown of C-bearing fluid after entrapment. In particular, breakdown of methane and subsequent diffusion of H out of the inclusions into point defects of the surrounding diamond host lattice seems a plausible explanation of this occurrence (see section 2.2.2.1). This process also accounts for efficient pressure relaxation between inclusion and host crystal. Other than for heavier atomic or molecular species for H_2, the diamond host lattice does not necessarily define a closed system. If we accept methane breakdown as origin of these inclusions, the pressure-temperature regime of their formation is constrained by the graphite-diamond phase boundary and the methane breakdown reaction. In subduction-zone environments or the mantle, decomposition of methane as component of C-H-O fluids depends on the activity of the fluid components (Stachel & Luth, 2015). However, the breakdown of encapsulated methane is constrained by pressure and temperature only, albeit that proton diffusion into the surrounding diamond lattice may affect mass balance. The relation between methane breakdown and plausible P-T regimes for formation and ascent of the host diamond is shown in Figure 2.1b: Plausible P-T points are defined through the intersection of the breakdown reaction (Lobanov et al., 2013) and the pressure-temperature evolution in a cold slab at 14 GPa, 1255 K as upper pressure bound, with the conditions of a hot slab at 5.7 GPa, 1350 K as lower bound or with the graphite-diamond boundary at 4.6 GPa, 1360 K as ultimate lower bound. Both lower bound estimates require interpolation of the decomposition line to conditions where experimentally mixtures of diamond, hydrogen, and higher alkanes had been observed (dashed blue line in Figure 2.1b; Lobanov et al., 2013). These constraints have to be placed into context with information from other inclusions in the same diamond to turn into a useful assessment of P-T paths. Currently, there is no good account how these occurrences of fine-grained diamond inclusions relate to type and origin of their host diamonds and about their abundance, because it requires synchrotron microdiffraction to detect these polycrystalline diamond inclusions within diamonds.

Graphite is a common inclusion in natural diamonds. In many cases chemically distinct inclusions in diamond are surrounded by graphitic damage zones, thus resulting in an optically dark appearance of these inclusions independent of their intrinsic optical absorption of visible light (Harris & Vance, 1972). Graphite and its occurrence in diamond as retrograde transformation product (Harris & Vance, 1972) are not within the scope of this chapter. We note that carbon phases of structure and bonding intermediate between graphite and diamond (Mao et al., 2003; Oganov et al., 2013) are suspected to occur also in such damage zones in diamonds but have not yet been firmly proved to exist in nature.

2.2.2. Carbides: Possible Indicators of Reducing Conditions in the Transition Zone and Lower Mantle

2.2.2.1. Methane

Methane is a component of C-H-O rich fluids in the mantle that are related to diamond formation (Stachel & Luth, 2015). Possible mechanisms are discussed in other chapters of this book. Here we focus on indications for methane or methane-bearing phases as crystalline inclusions in diamond. Methane crystallizes at 89.7 K in an fcc lattice (Hemley & Dera, 2000; Press, 1972), which at 8 GPa, 300 K, undergoes major structural rearrangement into a larger cubic structure with carbon atoms equivalent to those of α-Mn (Maynard-Casely et al., 2014). This high-pressure phase is called "methane B." This phase of methane appears to be stable to at least 25 GPa (Maynard-Casely et al., 2014). However, on Earth methane as solid phase is commonly found as clathrate with H_2O: Methane hydrates I and II are typical clathrate structures with van der Waals forces confining the methane guest molecule within the H-bonded ice network (Hemley & Dera, 2000; Loveday & Nelmes, 2008) and are abundant in permafrost soils and at the slope of continental shelfs (Kvenvolden, 1993). Above 2.4 GPa a different crystalline phase in the methane-water system replaces these clathrates (Loveday et al., 2001a, 2001b; Machida et al., 2007). Methane-hydrate III is a so-called "stuffed ice" (Loveday et al., 2001b): Other than in the clathrates, there is H

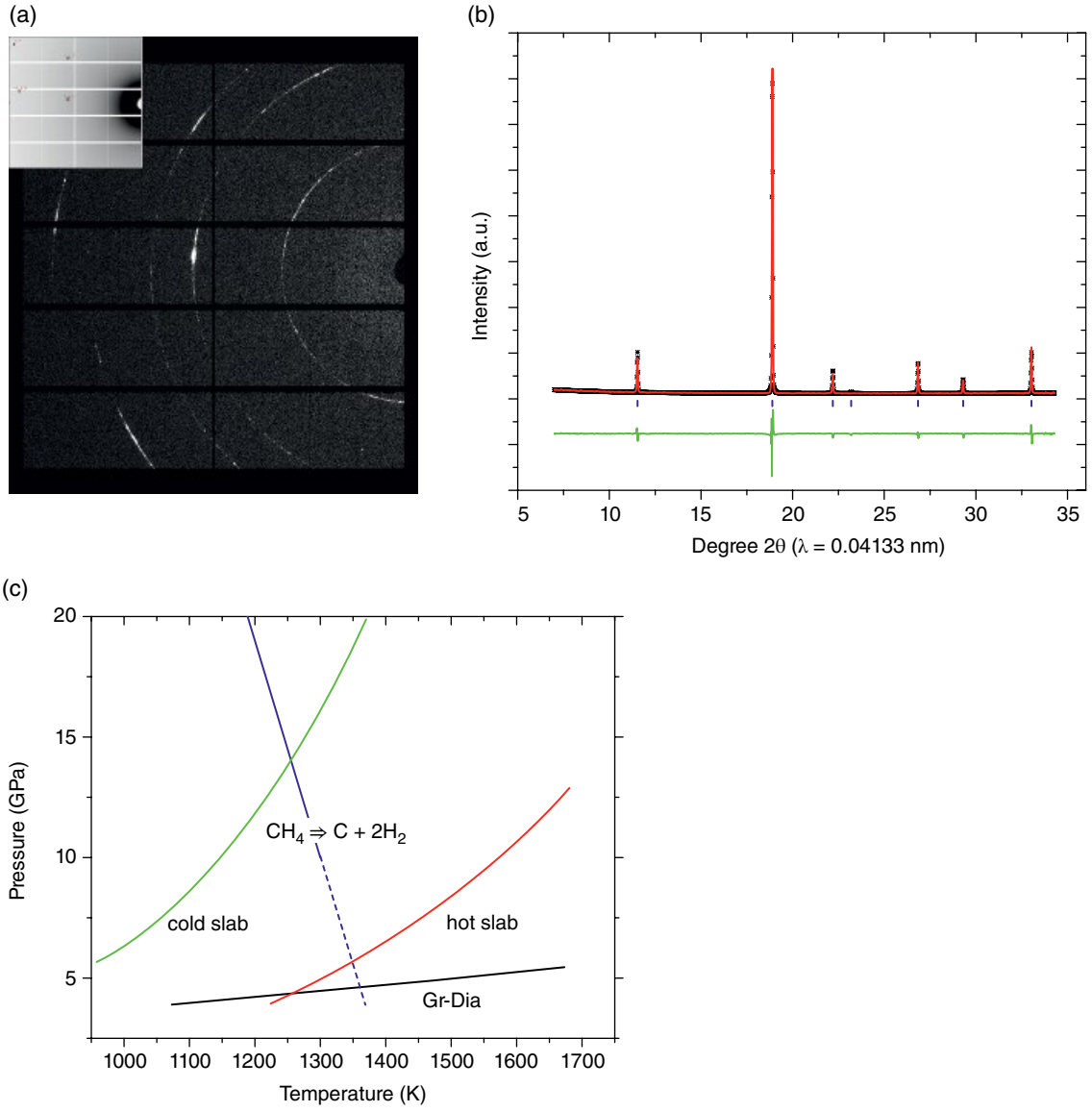

Figure 2.1 (a) Diffraction image of polycrystalline diamond within a single crystal diamond from Orapa, Botswana. The diffraction image was obtained during an overview diffraction map with $2 \times 4\,\mu m^2$ focused x-ray beam of 0.4133 Å wavelength at beamline 13-IDD, GSECARS, APS, Argonne National Laboratory. A Pilatus CdTe detector was used for data acquisition. In order to discriminate the diffraction signal from the intense elastic and inelastic diffuse scattering of the host diamond, an inclusion-free frame from within 20 µm distance from the inclusion was subtracted from this diffraction frame. Thus, the Bragg reflections from the host diamond are not visible. The strong texture of the polycrystalline diamond inclusion is clearly visible as intensity variation along the Debye fringes. Inset: Diffraction image before background frame subtraction. The single crystal diamond reflections are clearly visible. (b) Integrated diffraction pattern (black crosses) along with a whole profile refinement (red line) and residual of fit (green line). Bragg angles of diamond reflections are indicated as tickmarks. No excess pressure beyond a 0.1 GPa uncertainty is measurable. (c) Relation of the methane breakdown reaction (Lobanov et al., 2013) with the graphite-diamond phase boundary and pressure-temperature conditions in cold and hot subducted slabs (after Thomson et al., 2016). Intersection points mark possible conditions for diamond growth and ascent but additional geobarometric and thermometric constraints are necessary to determine which regime has actually occurred. See electronic version for color representation of the figures in this book.

bonding between methane and H_2O. The resulting structure is much denser than methane-hydrate I or II and can be well described as a distorted ice-Ih structure with methane molecules residing in the channels of this structure (Loveday et al., 2001b). Structures and properties of methane-hydrates are described in detail by Loveday and Nelmes (2008).

As of yet, direct evidence for methane in diamond comes from gas release into mass spectrometers upon crushing diamond specimens and from optical spectroscopy. E. Smith et al. (2015, 2016, 2018) reported Raman shifts of C-H bands at 2914 cm^{-1} and assigned them to methane. Infrared spectroscopy of diamonds shows frequent occurrence of C-H absorption bands that are related to alkanes (Navon, 1989) within the frequency range of 2915–3000 cm^{-1} (Figure 2.2). A frequently observed, additional C-H absorption band at 3107 cm^{-1} is assigned to protons that were trapped on nitrogen-related point defects in the diamond lattice and formed a chemical bond with N (Goss et al., 2014). This band is very sharp, consistent with an isolated chemical bond that allows for slowly decaying phonon states separated from the energy range of diamond phonons (defect band).

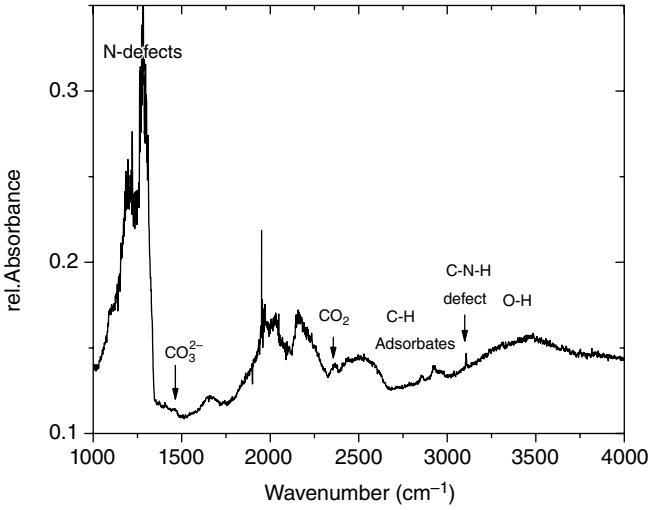

Figure 2.2 Infrared transmission spectrum of a doubly polished platelet of a fibrous diamond from Orapa, Botswana. The spectrum was taken from the fibrous rim of the specimen with 60×80 μ m^2 slits with 1.5 cm^{-1} spectral resolution at beamline 1.4, ALS, LBNL, Berkeley and has not been reported previously. The most prominent absorption feature are N-defect bands at 1000–1300 cm^{-1} and bands from two phonon processes of the regular diamond lattice between about 1800 and 2600 cm^{-1}. C-O, C-H, and O-H related bands are indicated. The energy of the "nu"$_3$ (C-O asymmetric stretching band) of CO_2 at 2365(1) cm^{-1} corresponds to 2.7(2) GPa, based on the pressured dependence of this mode in solid CO_2 (Hanson & Jones, 1981). Similarly, the carbonate asymmetric stretching mode at 1465 cm^{-1} corresponds to an elevated pressure, but the interpretation is less straightforward than for solid CO_2. For instance, for dolomite the energy of this band corresponds to a pressure around 2–3 GPa (Efthimiopoulos et al., 2017), but for calcite it is ~1 GPa (Koch-Mueller et al., 2016). See electronic version for color representation of the figures in this book.

IR-spectra of diamonds often show multiple bands around 2850–2950 cm^{-1}. These bands are related to surface contamination rather than to hydrocarbon inclusions within diamond (Navon, 1989).

Bands in the 2950 to 3050 cm^{-1} range can be assigned to methane at ambient pressure to several GPa or to other hydrocarbons at ambient to elevated pressures. Further studies are required to understand the state and the residual pressure of CH_4 in diamond. While methane is a likely component of diamond-forming fluids (see review by Shirey et al., 2013), it is important to know if C-H bands in diamond adhere to free alkanes and at which residual pressures they occur, or are bound to water as clathrates. We mentioned above that occurrences of fine-grained diamond inclusions within single crystal diamond can be interpreted as result of breakdown of entrapped methane (Figure 2.1).

2.2.2.2. Transition Metal Carbides and Carbonaceous Iron

Carbides of transition metals, notably of Fe, have been reported as rare occurrences in diamonds (Bulanova et al., 2010; Jacob et al., 2004; Kaminsky & Wirth, 2011; Mikhail et al., 2014). Mikhail et al. (2014) and E. Smith et al. (2016) found indications that these occurrences are not exotic anomalies. Inclusion of iron and iron carbides are plausibly connected with the formation process of sublithospheric diamonds and in particular with the formation of CLIPPIR, a specific type of diamonds (E. Smith et al., 2016). Tschauner et al. (2018) observed inclusions of carbonaceous iron in a number of diamonds of different origin and observed that some of these inclusions maintain high residual pressures, similar to inclusions of ice-VII, ilmenite, and calcite, reported in the same study.

The particular interest in iron and iron-carbide inclusions comes from their potential role in deep carbon recycling. In an experimental study Rohrbach and Schmidt (2011) found indication that diamond formation, carbon subduction, and the depth dependence of the mantle redox state are intrinsically connected. It is generally assumed that the mantle becomes more reducing with increasing depth. In the shallow upper mantle the dominant oxidation state of iron is 2+. Pressure in the range of tens of GPa favors disproportionation of ferrous iron into ferric and metallic iron (Frost et al., 2004; Frost & McCammon, 2008). Garnet inclusions in sublithospheric diamonds exhibit overall higher amounts of ferric iron (as skiagite) (Kiseeva et al., 2018) in consistency with the experimental studies. Rohrbach and Schmidt (2011) proposed that native iron in the transition zone and lower

mantle reacts with carbonate from fluids that are released from subducted slabs. The reaction results in formation of diamond and iron carbides. Consequently, inclusions of iron and iron carbides in diamond are not reflecting unusual processes but may be remnants of this "redox freezing" process.

The solubility of carbon in iron varies largely with temperature and structure. Pressure on the scale of several 10 GPa was found to suppress solubility (Lord et al., 2009). Pressure also affects the stability field of iron carbides and favors different stoichiometries than does ambient pressure (Lord et al., 2009). The carbon-rich side of the iron-carbon phase diagram at high pressure has been studied extensively in relation with the search for the light element in the Earth's out core (Lord et al., 2009; Dasgupta & Hirschmann, 2010, Chen et al., 2014). The iron-rich side of the Fe-C phase diagram is well known at ambient pressure, but little work has been dedicated to it at elevated pressure (Narygina et al., 2011). In nature, iron carbides have been found in meteorites (see review by Rubin & Ma, 2017), in terrestrial volcanites whose conduit intersected coal deposits (Irmer, 1920), in fulgurites (Essene & Fisher, 1986), and as inclusions in diamond (Jacob et al., 2004; Kaminsky & Wirth, 2011; Mikhail et al., 2014; E. Smith et al., 2016). As the other occurrences do not involve pressures on a GPa level, we only discuss the occurrences in diamond.

Cohenite, Fe_3C, has been found in diamonds (Jacob et al., 2004; Mikhail et al., 2014; E. Smith et al., 2016). Kaminsky and Wirth (2011) also reported haxonite, $Fe_{23}C_6$, and di-iron-carbide as inclusions in diamonds from Juina, Brazil. Occurrence of cohenite places a possible constraint on P-T conditions of entrapment: Pressures above 8 GPa favor formation of Fe_7C_3 at high carbon activity (Lord et al., 2009). Thus, cohenite has either been entrapped at lower pressures or formed upon retrograde transformation from Fe_7C_3 where excess carbon was resorbed by the surrounding diamond. E. Smith et al. (2016) reported occurrences of inclusions with taenite and cohenite intergrowth in CLIPPIR diamonds. In this case, Fe is in excess, and cohenite is exsolution product of a more carbonaceous alloy or melt, whereas the surrounding diamond was not significantly involved in formation of these phases other than through methane formation. Smith et al. argue that the cohenite-iron inclusion point to formation of the host diamonds in the deep transition zone because they observe in other CLIPPIR diamonds majoritic garnets and calcium silicate phases that are possible retrograde transformation products of $CaSiO_3$-perovskite (E. Smith et al., 2016).

This study as well as earlier observations of taenite and cohenite (Jacob et al., 2004; Kaminsky & Wirth 2011; Mikhail et al., 2014) are based on analyses of inclusions exposed by cutting or FIB milling.

A different approach was chosen recently by Tschauner et al. (2018) using in-situ synchrotron micro-X-ray diffraction and X-ray fluorescence spectroscopy for detection and identification of submicroscopic inclusions. While this work was primarily aiming to examine former fluid-inclusions in diamonds such as ice-VII, the same method also allowed for identifying micrometer-scale inclusions of other minerals, including iron, iron-nickel, and Fe-carbides (Tschauner et al., 2018). As in the case of ice-VII, in-situ micro-XRD allows for assessing the residual pressure of these inclusions and reconstructing the pressure and temperature of their entrapment based on nearly isochoric release paths (Navon 1991, 2017; Tschauner et al., 2018) or isomekes (Angel et al., 2014; Nasdala et al., 2003). In most cases the iron and carbide inclusions detected by synchrotron micro-X-ray diffraction and fluorescence resided at pressures below 1 GPa, but a smaller set of inclusions was found at residual pressures of 1 to 7 GPa. These rather high residual pressures are also consistent with the redox-freezing model, although it has to be noted that presently other pathways of reduction of ferrous or ferric species as side-product of reduction of carbonate to carbon cannot be excluded. For instance, ice-VII inclusions in diamonds are remnants of diamond-forming fluids, but probably they do not represent the bulk composition of those fluids (Tschauner at al., 2018).

We note that both taenite (fcc-iron, γ-iron) and iron (bcc-iron, α-iron) are observed, although so far only in different host diamonds. For clarification we recall here that mineral names are defined by structure and composition of the dominant endmember (Nickel & Grice, 1998). For taenite, this endmember is iron in fcc structure, although taenite usually contains few to several at% Ni (Rubin & Ma, 2017). For iron, the endmember is also Fe but in bcc structure, although in many natural occurrences it contains noticeable amounts of Ni ("kamacite"). In synchrotron micro-X-ray fluorescence measurements, I found that taenite inclusions in diamond contain Ni at levels of few to 30 at%, but iron contains ~1 at% Ni or less. However, this observation is based on about a dozen occurrences and it is not clear if this holds as a general pattern for iron inclusions in diamond.

In this context we note that "hcp-Fe" (ε-Fe) has actually been found in serpentinized peridotites and CAIs (calcium-aluminum-rich inclusions in chondrites) and is an approved mineral with the name hexaferrum (Mochalov et al., 1998; Rubin & Ma, 2017). In both types of occurrences hexaferrum is stabilized at ambient conditions through high amounts of Ir and Ru. So far, it has not been reported as inclusion in diamonds, where it would define release from lower mantle conditions.

The carbon-content of μ m-scale inclusions of taenite and iron is hard to assess through microchemical analysis.

However, the same structural distortion as in synthetic carbonaceous iron and iron-nickel is observed for many of these iron-metal inclusions, and Rietveld refinement of relative electron density at nonequivalent lattice sites is consistent with the presence of a light element. The saturation limit of C in fcc-iron and Fe-Ni has been examined by Narygina et al. (2011) and was found to be <0.9 at% at 9 GPa beyond which cohenite exsolution occurs upon cooling. The C content of iron has been found to be <4at% at 9 GPa, above which cohenite exsolution occurs, whereas at 20 GPa exsolution occurs at lower concentrations (Narygina et al., 2011). SEM-EDS analyses of exposed iron inclusions do not indicate the presence of Si. An example of a diffraction pattern of iron as diamond inclusion is given in Figure 2.3. We note that the iron inclusions in diamonds that we identified were always fine grained and textured. The d-spacings of a few single crystal reflections in the same pattern can be matched to cohenite and similar patterns with smooth powder-like iron patterns, and a few spots of d-spacings that match cohenite have been observed several times. Although the occurrence of diffraction features in the same diffraction image does not strictly imply coexistence, we note that the intergrowth of taenite with cohenite reported by E. Smith et al. (2016) generates an equivalent kind of diffraction patterns. Isolated inclusions of cohenite were generally found to be more coarse grained (few crystallites on micrometer scale within one inclusion) and consistently at pressures below 1 GPa. This low to ambient residual pressure may be owed to inelastic deformation and cracking of the host diamond around the carbide inclusions. Cohenite has a much higher bulk modulus than fcc- or bcc-iron (Chen et al., 2014), and a nearly isochoric release path from the conditions of the transition zone would imply much higher residual pressures than for metallic iron. We recall that some occurrences of cohenite in diamond may be products of the backreaction of Fe_7C_3, in which case the condition of a nearly conserved inclusion volume did not avail and the present state is the result of pressure release upon backreaction.

Finally, we note that other carbides have been found in concentrates from ultra-high-pressure terrains such as the Luobusha complex in Tibet. In particular, qushongite (WC), yarlongite, and tongbaite (Cr_3C_2) have been reported (Fang et al., 2009; Shi et al., 2009). The actual mechanism of their formation is not clear but their occurrence in rocks that have been obducted from deep lithospheric or even sublithospheric mantle (Dobrzhinetzkaya et al., 2009) justifies their mentioning here. It is also noteworthy that tantalcarbide (Ta,Nb)C was found in placers in the Ural mountains already at the beginning of the 20th century (originally interpreted as native Ta; von John, 1910), where possible synthetic origin can be precluded. Although tantalcarbide and niobocarbide (Jedwab, 2009) are derived from orogenic mantle peridotites, they are not necessarily mantle minerals. Formation under reducing conditions at low pressure during serpentinization cannot

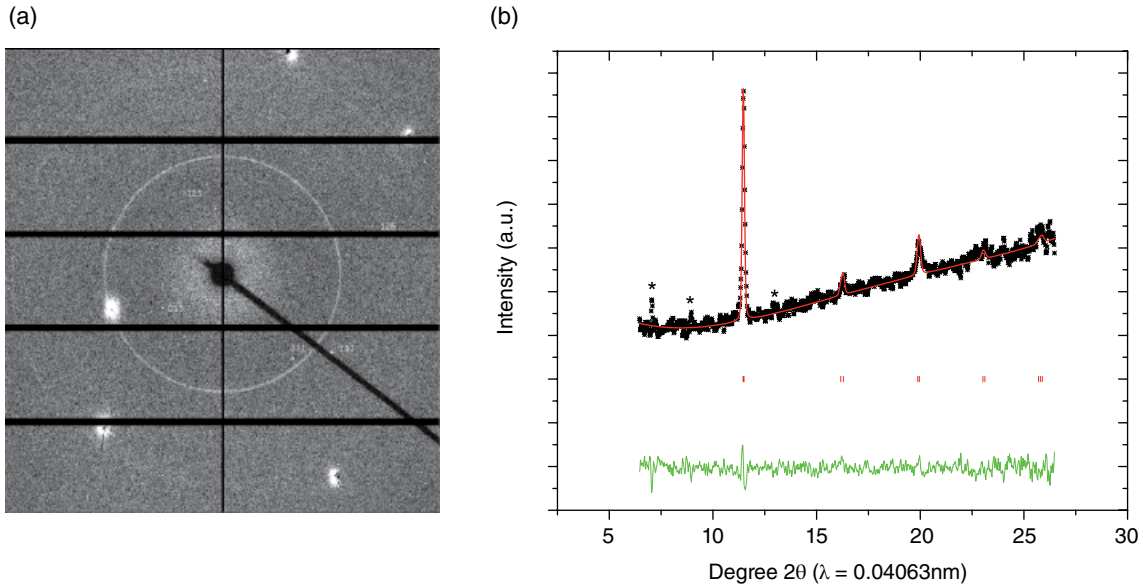

Figure 2.3 (a) Diffraction image of suessite as inclusion in a diamond from Orapa, Botswana. The image was obtained and treated in the same way as the one shown in Figure 2.1. Few isolated indexed single crystal reflections match cohenite. (b) Integrated diffraction pattern (black) with Rietveld refined modeled pattern of tetragonally distorted iron (red) and residual of fit (green). Bragg angles of allowed reflections are indicated by tickmarks. See electronic version for color representation of the figures in this book.

be excluded in absence of additional information about their content of trace elements and carbon isotopes.

2.3. OXIDES AND CARBONATES

As in the case of carbonaceous iron and iron carbides, the occurrence of CO_2 and carbonates as inclusions in diamonds bears witness of the formation process of diamond and the process of carbon recycling in the mantle. Extensive studies on carbonaceous fluid inclusions in diamonds (Izreali et al., 2001; Jablon & Navon, 2016) and experimental work on carbonate and carbonate-rich silicate melts have been conducted (Litasov et al., 2011; Podnorodnikov et al., 2001) to the purpose of elucidating these processes. Both molecular carbon dioxide and carbonate were detected in diamond by means of their characteristic absorption bands in transmission infrared spectroscopy (Navon, 1991). The energy of the band related to asymmetric stretching of the carbonate C-O bond ranges from 1430 to 1445 cm^{-1}. Frequently, a doublet or multiplet is observed (Navon, 1989; see also Figure 2.3), which indicates either carbonate inclusions at different residual pressures or of different composition and structure. In addition, a carbonate C-O bending mode is observed at 876 ± 1.5 cm^{-1} shifted to 878 to 879 cm^{-1} in diamonds where the carbonate C-O stretching band is shifted to 1445 cm^{-1} (Navon, 1989), which is consistent with elevated residual pressure in the GPa-range. We discuss the residual pressure of carbonate inclusions in diamonds further below.

2.3.1. Carbon Dioxide

Carbon dioxide exhibits a large variety of phases at different pressures and temperatures (Iota et al., 1999, 2007; Tschauner et al., 2001; Datchi et al., 2009, 2012, 2014; Litasov et al., 2011; Santoro et al., 2012). CO_2 crystallizes as dry ice (CO_2-I) at 194.5 K and ambient pressure and becomes stable at ambient temperature at 0.5 GPa (Bridgman, 1914). The structure is an fcc-like arrangement of CO_2 molecules (Simon & Peters, 1980) whose librational modes stabilize the cubic lattice. At pressures in the GPa range, CO_2 undergoes a transition to a metastable low-symmetric arrangement of molecules (CO_2-II) which transforms to orthorhombic CO_2-III at ~ 10 GPa (Aoki et al., 1994). This spontaneous structural distortion is a result of the suppression of librational modes upon compression. At above 23 GPa and temperatures above 2000 K, CO_2 assumes a crystalline network structure, CO_2-V. This drastic change in structure and chemical bonding was first observed by Iota et al. (1999) by means of Raman spectroscopy and subsequently characterized as formation of a cristobalite-like structure (Datchi et al., 2012; Santoro, 2012). In the intermediate pressure-temperature regime between the stability field of CO_2-I and CO_2-V, a variety of different phases has been observed with little consistency in structure and stability fields (Datchi et al., 2012, 2014; Iota et al., 1999, 2007; Santoro et al., 2012). This includes different reconfigurations of molecules to denser packing (Datchi et al., 2012, 2014) as well as, possibly, unbent CO_2 molecules in a rutile-like arrangement (Iota et al., 2007). Various studies (Tschauner et al., 2001; Takafuji et al., 2006; Litasov et al., 2011) found that above 25–30 GPa, CO_2 decomposes along a negative Clapeyron slope that intersects the present average mantle geotherm between 900 and 1100 km depth. Given the range of residual pressures found in diamond inclusions (Navon, 1991; Schrauder & Navon, 1993; Tschauner et al., 2018), CO_2-I,-II, -III, and -IV may occur as inclusions in diamond.

Both bending and asymmetric stretching related bands of molecular CO_2 were observed, often in diamonds that also contain carbonate. Interestingly, the IR absorption band of the vibron (that is: the C-O asymmetric stretching vibration of molecular CO_2) of CO_2 in diamonds has an energy of around 2350 cm^{-1} or higher (2365 cm^{-1} in the example given in Figure 2.3) and is usually split. This energy is noticeably above the vibron energy of dry ice (CO_2-I) at ambient pressure (interpolated to 300 K; Hanson & Jones, 1981). The splitting of the vibron indicates its interaction with other phonon states and is also characteristic for CO_2 phases at elevated pressure (Hanson & Jones 1981). It was noticed that at least in some cases, the CO_2 bending mode energies do not match the the energies of the vibron for any pressure and any known phase of CO_2 (Hainschwang et al., 2008). A possible explanation is that CO_2 is not occurring as free phase but captured in a clathrate or "filled ice." Currently, there is no diffraction-based structural information about this dense CO_2 or CO_2-bearing phase.

In general, the vibron energy is a good scale of pressure as it is rather independent on the structural configuration of CO_2 molecules, due to its nature as intramolecular vibration (Hanson & Jones, 1981). Consequently, Navon (1991) and Schrauder and Navon (1993) used this information to estimate current residual pressure of CO_2-bearing inclusions. In a second step, they estimated the conditions of entrapment of CO_2 based on isochoric paths that connect the current residual pressure and temperature with the pressure and temperature of entrapment. They obtained pressures of between 4 and 7 GPa where these isochores of CO_2 intersect plausible geotherms of the lithospheric mantle underneath the localities of the CO_2-hosting diamonds. Hereby they assumed that CO_2 forms a phase by itself. These pressures and temperatures are at the upper limit of CO_2 stability in eclogite (Thomson et al., 2016). CO_2 as inclusion in diamond does not necessarily represent high CO_2 concentrations in diamond-forming environments but may

represent a transient state or by-product of the breakdown of carbonate and subsequent diamond formation: Forming diamond can trap reaction educts and transient products as inclusions. For instance, methane and molecular hydrogen have been observed as inclusions in synthetic diamonds (E. Smith & Wang, 2016) and ice-VII inclusions in natural sublithospheric diamonds are likely such by-products of diamond formation during fluid-rock interaction rather than implying presence of an H_2O-dominated fluid (Tschauner et al., 2018).

2.3.2. Carbonates

Calcite, magnesite, siderite, eitelite $Na_2Mg(CO_3)_2$, nahkolite $NaHCO_3$, shortite $Na_2Ca_2(CO_3)_3$, and nyerereite $Na_2Ca(CO_3)_2$ have been observed as inclusions in diamonds. While these minerals are not genuinely high-pressure phases, it has been argued that they have formed in the mantle along with their host diamonds. Infrared absorption bands of some carbonate inclusions in diamond are consistent with elevated sustained pressures (Figure 2.3). Recently, a magnesian calcite inclusion at a residual pressures of 8.5±0.5 GPa was reported (Tschauner et al., 2018). This direct as well the indirect petrographic evidence for carbonate formation at pressures of several GPa makes it important to discuss these occurrences here. We start with nonquenchable high-pressure polymorphs of these carbonates, which have not yet been observed but may occur as inclusions in diamonds; then we briefly summarize observed occurrences of carbonate inclusions and conclude with the reconstruction of the entrapment conditions of a high-pressure calcite inclusion in a diamond.

Pure calcite undergoes a sequence of transformations to high-pressure structures: At 2 GPa, calcite undergoes a distortive transition to calcite-II (Merill & Bassett, 1975), which at 4 and 9 GPa transforms to calcite-III and calcite-IV, respectively, both of which assume very different configurations of Ca and carbonate groups (Merlini et al., 2012, 2014), though they can still be considered as highly distorted NaCl-type lattices, like calcite itself. At elevated temperature and pressure, calcite transforms to aragonite, which itself undergoes structural transitions upon compression (Oganov et al., 2006, 2008; D. Smith et al., 2018). As pure phases, magnesite and dolomite appear to be stable up to pressures in the 70–80 GPa range (Fiquet et al., 1994; Oganov et al., 2006, 2008, 2013; Pickard & Needs, 2015).

In principle, calcite-II, -III, -IV, aragonite, and postaragonite may be expected as inclusions in diamonds over the pressure range that has been found for CO_2 (Schrauder & Navon, 1993), ice-VII (Tschauner et al., 2018), magnesian calcite, and ilmenite (Tschauner et al., 2018), but none of these phases of $CaCO_3$ has been observed so far; the principal reason is the Mg content of calcite entrapped in diamond. The magnesite component stabilizes the calcite structure due to its high negative excess volume (Redfern & Angel, 1999; Buob et al., 2006). With increasing pressure of the calcite inclusions, an increase of Mg content is observed to levels where calcite-dolomite segregation occurs at low pressure. Experimental studies indicate that dolomite, magnesite, and Na carbonates replace calcite as stable carbonate phase in eclogite over pressures of 3 to above 15 GPa (Thomson et al., 2016), but inclusions in diamond may be more enriched in less compatible elements such as Ca over Mg or K over Na.

Siderite has been observed as inclusion of diamond but at nearly ambient pressure. Hence, it may be a precipitate at a crack. This also holds for numerous occurrences of Mg-poor calcite whose residual pressure is ambient or nearly ambient.

Studies based on Raman spectroscopy and electron microscopy (Bulanova et al., 2010; Kaminsky et al., 2009; Kaminsky & Wirth, 2011) have found a number of alkaline carbonates as inclusions in diamond, which highlights the role of carbonaceous melt in formation and growth of diamonds. These minerals are eitelite $Na_2Mg(CO_3)_2$, nahkolite $NaHCO_3$, shortite $Na_2Ca_2(CO_3)_3$, and nyerereite $Na_2Ca(CO_3)_2$, which have also been found as fluid inclusions in olivine xenocrysts from kimberlites (Golovin & Sharygin, 2007) and appear to have stability fields in carbonaceous melts in the range of a few GPa (Podnorodnikov et al., 2018). These carbonates are also found in carbonatitic volcanites. Sodic carbonates can also form at much higher pressure in eclogitic paragenesis (Thomson et al., 2017).

So far, residual pressures of calcite inclusions have been found to range between 1 and 9 GPa. Figure 2.4a shows the diffraction pattern of one of these inclusions (Tschauner et al., 2018). The composition is $(Ca_{0.75(2)}Mg_{0.25(2)})CO_3$. As described in Tschauner et al. (2018), the residual pressure can be estimated based on the compositional dependence of the bulk moduli and volumes of carbonates in the calcite and dolomite series (Redfern & Angel, 1999). Thermoelastic parameters were calculated by a combination of ab-initio and finite-temperature methods. The residual pressure was corrected for elastic relaxation of the surrounding diamond (Angel et al., 2014). This corrected pressure was used as endpoint of a quasi-isochoric release path, where volume changes of the diamond were taken into account (Tschauner et al., 2018). Figure 2.4 shows the upper and lower bound of the release path. The path intersects the solidus of carbonated MORB around its maximum between 11 and 13 GPa (Thomson et al., 2017). This pressure-temperature regime is a plausible upper bound for entrapment of the carbonate and diamond formation. With this tentative fix point, the limits of the entrapment path of magnesian

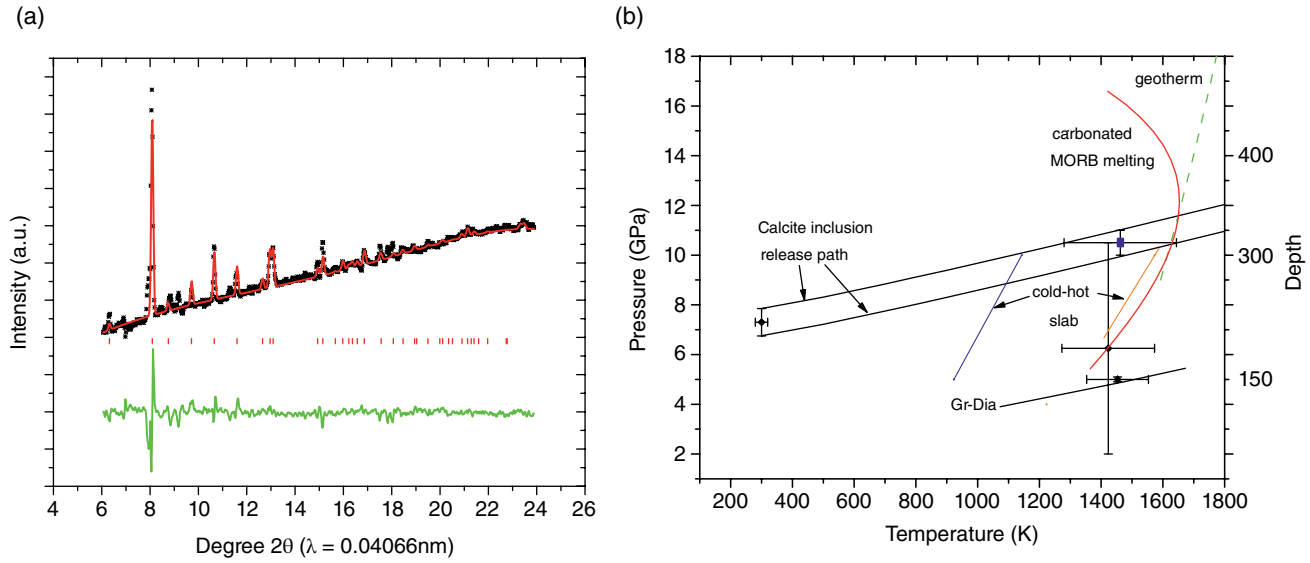

Figure 2.4 (a) Integrated diffraction pattern (black crosses), Rietveld refined calcite model pattern (red line), and residual of fit (green line) of a magnesian calcite inclusion in a cloudy diamond from Shandong, China (after Tschauner et al., 2018, Supplement). Tick marks indicate the Bragg angles of allowed reflections of calcite. The Rietveld refinement was used to determine unit cell parameters and Ca/Mg ratio. The phase contrast between Ca and Mg is sufficiently large to constrain this ratio to within 8% of the Mg content. (b) Reconstruction of entrapment conditions of this magnesian calcite. Black lines: Upper and lower bound of the release path for the inclusion. The possible breakdown of magnesian calcite into dolomite and magnesite (Buob et al., 2006) is not considered. Black diamonds: current residual pressure corrected for elastic relaxation of diamond (Tschauner et al., 2018), geobarometric and geothermometric estimate of growth of clinopyroxene with ilmenite exsolution lamellae (Gao et al., 2008), estimate of entrapment of an olivine inclusion in a diamond from the same area (Yin et al., 2017). Red line: solidus of carbonated MORB (Thomson et al., 2016); blue and orange lines: bounds for cold and hot subduction (after Thomson et al., 2016). Dashed green line: average mantle reference geotherm (after Brown & Shankland, 1981). See electronic version for color representation of the figures in this book.

calcite define a range of 1300 to 1650 K and 11 to 13 GPa, just above the boundary between upper mantle and transition zone. We compare this result with an estimate of pressure-temperature regime based on ilmenite exsolution in clinopyroxenes (Gao et al., 2008) and an independent estimate of entrapment conditions of an olivine crystal in diamond (Yin et al., 2017). The geobarometric estimate from ilmenite exsolution in clinopyroxene varies significantly between a minimal pressure of 2 GPa and 8 GPa and temperatures of 1300 to 1600 K. The estimated entrapment of an olivine inclusion does not provide an uncertainty in pressure. The three data points taken together constrain pressures and temperatures of subduction and ascent of material such as subduction to 11–13 GPa or deeper, release of carbonate-rich melt and subsequent melting of shallower peridotitic mantle, in agreement with scenarios that have been proposed for the North China Craton from geochemical data (Gao et al., 2008). However, reconstruction of entrapment conditions of diamond inclusions (Figure 2.4b; Yin et al., 2017) along with geobarometric estimates promise better constraints on the actual P-T conditions of these different steps.

CONCLUSION

Carbonaceous mineral inclusions at high residual pressures and high-pressure carbonaceous minerals provide important constraints on formation of diamond and the deep carbon cycle of Earth. Both reduced carbonaceous species, such as carbides, and oxidized species, such as carbonates, allow for correlating experimental petrological constraints on formation and stability with actual occurrences of carbonates and carbides in deep, diamantiferous mantle. As of yet, diamond, methane, transition metal carbides, CO_2, and various carbonates have been found either directly as minerals through microchemical and microstructural analysis, or have been detected through optical spectroscopy of inclusions in diamonds. The actual structural state of CH_4 and CO_2 either as pure phases as inclusions or as clathrates or icy phases is not yet known. Iron carbides, carbonaceous iron, and carbonate minerals have been identified. Some of these inclusions sustain still-high residual pressures, which can be used to reconstruct the pressures and temperatures of their entrapment. These results can be

combined with geochemical and geophysical modeling of processes in the mantle.

ACKNOWLEDGMENTS

The author would like to thank the two reviewers and the editor for their helpful comments. The author also acknowledges support through NSF-EAR 1838330. Data presented were obtained at beamlines 13-IDD, GeoSoilEnviroCARS (The University of Chicago), 16-IDC, HPCAT, Advanced Photon Source (APS), Argonne National Laboratory, and 1.4 at the Advanced Light Source, which is a DOE Office of Science User Facility under contract no. DE-AC02-05CH11231. HPCAT operations are supported by DOE-NNSA's Office of Experimental Sciences. GeoSoilEnviroCARS is supported by the National Science Foundation – Earth Sciences (EAR-1634415) and Department of Energy – GeoSciences (DE-FG02-94ER14466). The Advanced Photon Source is a U.S. Department of Energy (DOE) Office of Science User Facility operated for the DOE Office of Science by Argonne National Laboratory under Contract No. DE-AC02-06CH11357. The publication of this chapter and this monograph is supported through the Deep Carbon Observatory.

REFERENCES

Anders. E., & Zinner, E. (1993). Interstallar grains in primitive meteorites: Diamond, silicon-carbide, and graphite. *Meteoritics*, *28*(4), 490–514.

Angel, R. J., et al. (2014). Geobarometry from host-inclusion systems: The role of elastic relaxation. *American Mineralogist*, *99*(10), 2146–2149.

Aoki, K., et al. (1994).Crystal-structure of the high-pressure phase of solid CO2. *Science*, *263*(5145), 356–358.

Boyd, S. R., et al. (1994). Modelling the growth of natural diamonds. *Chemical Geology*, *116*, 29–42.

Brenker, F. E., et al. (2002). Exhumation of lower mantle inclusions in diamond: ATEM investigation of retrograde phase transitions, reactions and exsolution. *Earth and Planetary Science Letters*, *198*(1-2), 1–9.

Bridgman, P. W. (1914). Change of phase under pressure: I. The phase diagram of eleven substances with especial reference to the melting curve. *Physical Review*, *3*(3), 153–203.

Brown, J. M., & Shankland, T. J. (1981). Thermodynamic parameters in the Earth as determined from seismic profiles. *Geophysical Journal of the Royal Astronomical Society*, *66*(3), 579–596.

Bulanova, G., et al. (2010). Mineral inclusions in sublithospheric diamonds from Collier 4 kimberlite pipe, Juina, Brazil: Subducted protoliths, carbonated melts and primary kimberlite magmatism. *Contrib. Mineral. Petrol.*, *160*, 489–510.

Buob, A., et al. (2006) Experiments on CaCO3-MgCO3 solid solutions at high pressure and temperature. *American Mineralogist*, *91*, 435-440.

Chen, B., et al. (2014). Hidden carbon in Earth's inner core revealed by shear softening in dense Fe7C3. *Proceedings of the National Academy of Sciences of the United States of America*, *111*(50), 17755–17758.

Dana, J. D. (1869). *System of mineralogy*. 5th ed. New York: Wiley & Sons.

Dasgupta, R., & Hirschmann, M. M. (2010). The deep carbon cycle and melting in Earth's interior. *Earth and Planetary Science Letters*, *298*(1-2), 1–13.

Datchi, F. et al. (2009). Structure of carbon dioxide phase IV: Breakdown of the intermediate bonding state scenario. *Physical Review Letters*, *103*(18), Article Number: 185701.

Datchi, F. et al. (2012). Structure of polymeric carbon dioxide CO2-V. *Physical Review Letters*, *1089*(12), 125701.

Datchi, F. et al. (2014). Structure and compressibility of the high-pressure molecular phase II of carbon dioxide. *Physical Review B*, *89*(14), Article Number: 144101.

Dobrzhinetskaya, L. F., et al. (2009). High-pressure highly reduced nitrides and oxides from chromitite of a Tibetan ophiolite. *Proceedings of the National Academy of Sciences of the United States of America*, *106*(46), 19233–19238.

Efthimiopoulos, I., et al. (2017). Combined high-pressure and high-temperature vibrational studies of dolomite: Phase diagram and evidence of a new distorted modification. *Physics and Chemistry of Minerals*, *44*(7), 465–476.

El Goersy, A., & Donnay, G. (1968). A new allotropic form of carbon from Ries crater. *Science*, *161*(3839), 363.

El Goresy, A., et al. (2003). A new natural, super-hard, transparent polymorph of carbon from the Popigai impact crater, Russia. *Comptes Rendus Geoscience*, *335*(12), 889–898.

Essene, E. J., & Fisher, D. C. (1986) Lightning strike fusion: Extreme reduction and metal-silicate liquid immiscibility. *Science*, *234*(4773), 189–193.

Fang, Q., et al. (2009). Qusongite (WC): A new mineral, locality: Luobusa ophiolite, Qusong County, Tibet, China. *American Mineralogist*, *94*, 387–290.

Fiquet, G., et al. (1994). High-pressure X-ray diffraction study of carbonates: MgCO3, CaMg(CO3)2, and CaCO3. *American Mineralogist*, *79*, 15–23.

Frost, D. J., et al. (2004). Experimental evidence for the existence of iron-rich metal in the Earth's lower mantle. *Nature*, *428*(6981), 409–412.

Frost, D. J., & McCammon, C. A. (2008). The redox state of Earth's mantle. *Annual Review of Earth and Planetary Sciences*, *36*, 389–420.

Gao, S., et al. (2008). Recycling deep cratonic lithosphere and generation of intraplate magmatism in the North China Craton. *Earth and Planetary Science Letters*, *270*, 41–53.

Golovin, A. V., & Sharygin, V. V. (2007). Petrogenetic analysis of fluid and melt inclusions in minerals from mantle xenoliths from the Bele pipe basanites (North Minusa depression). *Russian Geology and Geophysics*, *48*(10), 811–824.

Goss, J. P., et al. (2014). Identification of the structure of the 3107 cm(-1) H-related defect in diamond. *Journal of Physics: Condensed Matter*, *26*(14), Article Number: 145801. doi: 10.1088/0953-8984/26/14/145801.

Hainschwang, T., et al. (2008). HPHT treatment of CO2 containing and CO2-related brown diamonds. *Diamond and Related Materials*, *17*(3), 340–351.

Hanson, R. C., & Jones, L. H. (1981). Infrared and Raman studies of pressure effects on the vibrational-modes of solid CO2. *Journal of Chemical Physics*, *75*(3), 1101–1112.

Harris, J. W., & Vance, E. R. (1972). Induced graphitization around crystalline inclusions in diamond. *Contributions to Mineralogy and Petrology*, *35*(3), 227–234.

Harte, B., et al. (1999). Lower mantle mineral associations in diamond crystals from Sao Luiz, Brazil. In Yingwei Fei, C. M. Bertka, & B. O. Mysen (Eds.), *Mantle petrology: Field observations and high pressure experimentation: A tribute to Francis R. (Joe) Boyd* (Spec. Publ. 6, pp. 125–153). The Geochemical Society.

Helffrich, G. R., & Wood, B. J. (2001). The Earth's mantle. *Nature*, *412*(6846), 501–507.

Hemley, R. J., & Dera, P. (2000). Molecular crystals. *Reviews in Mineralogy & Geochemistry*, *41*, 335–419.

Hough R. M., et al. (1995). Diamond and silicon-carbide in impact melt rock from the Ries impact crater. *Nature*, *378*(6552), 41–44.

Howell, D., et al. (2012). Inclusions under remnant pressure in diamond: A multi-technique approach. *European Journal of Mineralogy*, *24*(4), 563–573.

Iota, V., et al. (1999). Quartzlike carbon dioxide: An optically nonlinear extended solid at high pressures and temperatures. *Science*, *283*(5407), 1510–1513.

Iota, V., et al. (2007). Six-fold coordinated carbon dioxide VI. *Nature Materials*, *6*(1), 34–38.

Irmer, W. (1920). Der Basalt des Bühls bei Kassel und seine Einschlüsse von Magnetit, Magnetkies und gediegen Eisen. *Abhandlungen der Senckenbergischen Naturforschenden Gesellschaft*, *13*, 91–108.

Izraeli, E. S., et al. (2001). Brine inclusions in diamonds: A new upper mantle fluid. *Earth and Planetary Science Letters*, *187*, 323–332.

Jablon, B. M., & Navon, O. (2016). Most diamonds were created equal. *Earth and Planetary Science Letters*, *443*, 41–47.

Jacob, D. E., et al. (2004). Cohenite, native iron and troilite inclusions in garnets from polycrystalline diamond aggregates. *Contributions to Mineralogy and Petrology*, *146*(5), 566–576.

Jedwab, J. (1990). Native ruthenium in tantalum carbide concentrates from the Ural Mountains, USSR. *Mineralogy and Petrology*, *43*(2), 137–146.

Kaminsky, F. V., & Wirth, R. (2011). Iron-carbide inclusions on lower-mantle diamond from Juina, Brazil. *Canadian Mineralogist*, *49*(2), 555–572.

Kaminsky, F. V., & Wirth, R. (2017). Nitrides and carbonitrides from the lowermost mantle and their importance in the search for Earth's "lost" nitrogen. *American Mineralogist*, *102*(8), 1667–1676.

Kaminsky, F., Wirth, R., Matsyuk, S., Schreiber, A., & Thomas, R. (2009). Nyerereite and nahcolite inclusions in diamond: Evidence for lower-mantle carbonatitic magmas. *Mineralogical Magazine*, *73*(5), 797–816. doi: 10.1180/minmag.2009.073.5.797

Kiseeva, E. S., et al. (2018). Oxidized iron in garnets from the mantle transition zone. *Nature Geoscience*, *11*(2), 144–147.

Koch-Mueller, M., et al. (2016). Phase transitions in the system CaCO3 at high P and T determined by in situ vibrational spectroscopy in diamond anvil cells and first-principles simulations. *Physics and Chemistry of Minerals*, *43*(8), 545–561.

Kvenvolden, K. A. (1993). Gas hydrates: Geological perspective and global change. *Reviews of Geophysics*, *31*(2), 173–187.

Litasov, K. D., et al. (2011). Crossover from melting to dissociation of CO2 under pressure: Implications for the lower mantle. *Earth and Planetary Science Letters*, *309*(3–4), 318–323.

Lobanov, S. S., et al. (2013). Carbon precipitation from heavy hydrocarbon fluid in deep planetary interiors. *Nature Communications*, *4*, Article Number: 2446.

Lord, O. T., et al. (2009). Melting in the Fe-C system to 70 GPa. *Earth and Planetary Science Letters*, *284*(1–2), 157–167.

Loveday, J. S., et al. (2001a). Stable methane hydrate above 2 GPa and the source of Titan's atmospheric methane. *Nature*, *410*, 661–663.

Loveday, J. S., et al. (2001b). Transition from cage clathrate to filled ice: The structure of methane hydrate III. *Physical Review Letters*, *87*, 215501-1.

Loveday, J. S., & Nelmes, R. J. (2008). High-pressure gas hydrates. *Physical Chemistry Chemical Physics*, *10*(7) 937–950.

Ma, C. (2018). A closer look at shocked meteorites: Discovery of new high-pressure minerals. *American Mineralogist*, *103*(10), 1521–1522.

Machida, S.-I., et al. (2007). Raman-spectra of methane hydrate up to 86 GPa. *Physics and Chemistry of Minerals*, *34*, 31–35. doi 10.1007/s00269-006-0126-6.

Mao, W. L., et al. (2003) Bonding changes in compressed superhard graphite. *Science*, *302*(5644), 425–427.

Maynard-Casely H. E., et al. (2014). The crystal structure of methane B at 8 GPa: An α-Mn arrangement of molecules. *Journal of Chemical Physics*, *141*, 234313. doi: 10.1063/1.4903813.

Merrill, L., & Bassett, W. A. (1975). Crystal-structure of CaCO3(II), a high-pressure metastable phase of calcium-carbonate. *Acta Crystallographica Section B – Structural Science*, *31*, 345–350.

Merlini, M., et al. (2012). CaCO3-III and CaCO3-VI, high-pressure polymorphs of calcite: Possible host structures for carbon in the Earth's mantle. *Earth and Planetary Science Letters*, *333*, 265–271.

Merlini, M., et al. (2014). Evidence of interspersed co-existing CaCO3-III and CaCO3-IIIb structures in polycrystalline CaCO3 at high pressure. *Mineralogical Magazine*, *78*(2), 225–233.

Mikhail, S., et al. (2014). *Geochemistry Geophysics Geosystems*, *15*, 855–866.

Mochalov, A. G., et al. (1998). Hexaferrum (Fe, Ru) (Fe, Os) (Fe, Ir)-A new mineral. *Zap Vseross Mineral Obshch*, *127*, 41–51.

Nasdala, L., et al. (2003). Spectroscopic 2D-tomography: Residual pressure and strain around mineral inclusions in diamonds. *European Journal of Mineralogy*, *15*, 931–935. doi: 10.1127/0935-1221/2003/0015-0931.

Navon, O. (1989). Chemical and Mineralogical Characterization of Microinclusions in diamonds. PhD Thesis, California Institute of Technology 1989.

Navon, O. (1991). High internal pressures in diamond fluid inclusions determined by infrared-absorption. *Nature*, *353*(6346), 746–748.

Navon O., et al. (2017). Solid molecular nitrogen (delta-N-2) inclusions in Juina diamonds: Exsolution at the base of the transition zone. *Earth and Planetary Science Letters*, *464*, 237–247.

Narygina, O., et al. (2011). Phase relations in Fe–Ni–C system at high pressures and temperatures. *Physics and Chemistry of Minerals*, *38*, 203–214. doi 10.1007/s00269-010-0396-x.

Nemeth, P., et al. (2014). Lonsdaleite is faulted and twinned cubic diamond and does not exist as a discrete material. *Nature Communications*, *5*, Article Number 5447.

Nestola, F., et al. (2018). CaSiO3 perovskite in diamond indicates the recycling of oceanic crust into the lower mantle. *Nature*, *560*. doi:10.1038/nature25972.

Nickel, E. H., & Grice, J.D. (1998). The IMA commission on new minerals and mineral names: Procedures and guidelines on mineral nomenclature. *Canad. Min.*, *36*, 913–926.

Oganov, A. R., et al. (2006). High-pressure phases of CaCO3: Crystal structure prediction and experiment. *Earth and Planetary Science Letters*, *241*(1–2), 95–103.

Oganov, A. R., et al. (2008). Novel high-pressure structures of MgCO3, CaCO3 and CO2 and their role in Earth's lower mantle. *Earth and Planetary Science Letters*, *273*(1–2), 38–47.

Oganov, A. R., et al. (2013). Structure, bonding, and mineralogy of carbon at extreme conditions. Carbon in Earth,book series: *Reviews in Mineralogy, & Geochemistry*, *75*, 47–77.

Pearson, D. G., et al. (2014). Hydrous mantle transition zone indicated by ringwoodite included within diamond. *Nature*, *507*(7491), 221–223.

Pickard, C. J., & Needs, R. J. (2015). Structures and stability of calcium and magnesium carbonates at mantle pressures. *Physical Review B*, *91*(10), Article Number: 104101.

Press W. (1972). Structure and phase transitions of solid heavy methane (CD4). *Journal of Chemical Physics*, *56*, 2597.

Podborodnikov, I. V., Shatskiy, A., Arefiev, A. V., Bekhtenova, A., Litasov, K. D. (2019). New data on the system Na2CO3-CaCO3-MgCO3 at 6 GPa with implications to the composition and stability of carbonatite melts at the base of continental lithosphere. *Chemical Geology*, *515*, 50–60. doi:10.1016/j.chemgeo.2019.03.027

Redfern, S.A.T., & Angel, R. J. (1999). High-pressure behaviour and equation of state of calcite, CaCO3. *Contributions to Mineralogy and Petrology*, *134*(1), 102–106.

Rohrbach, A., & Schmidt M. W. (2011). Redox freezing and melting in the Earth's deep mantle resulting from carbon-iron redox coupling. *Nature*, *449*, 456–458.

Rubin A. E., & Ma. C. (2017). Meteoritic minerals and their origins. *Chemie der Erde – Geochemistry*, *77*(3), 325–385.

Santoro, M., et al. (2012). Partially collapsed cristobalite structure in the non molecular phase V in CO2. *Proceedings of the National Academy of Sciences of the United States of America*, *109*(14), 5176–5179.

Schrauder, M., & Navon, O. (1993). Solid carbon-dioxide in a natural diamond. *Nature*, *365*(6441), 42–44.

Schulte, P., et al. (2009). A dual-layer Chicxulub ejecta sequence with shocked car-bonates from the Cretaceous-Paleogene (K-Pg) boundary, Demerara Rise, western Atlantic. *Geochimica et Cosmochimica Acta*, *73*(4), 1180–1204.

Sharp, T. G., & DeCarli, P. S. (2006). Shock effects in meteorites. In *Meteorites and the Early Solar System II* (pp. 653–677). Tucson: University of Arizona Press.

Shi, N., et al. (2009). Yarlongite: A new metallic carbide mineral. *Acta Geologica Sinica – English Edition*, *83*(1), 52–56.

Shirey, S. B., et al. (2013). Diamonds and the geology of mantle carbon. Carbon in Earth, book series: *Reviews in Mineralogy, & Geochemistry*, *75*, 355–421.

Simon, A., & Peters, K. (1980). Single-crystal refinement of the structure of carbon-dioxide. *Acta Crystallographica Section B – Structural Science*, *36*, 2750–2751.

Smith, D., et al. (2018a). Postaragonite phases of CaCO3 at lower mantle pressures. *Physical Review Materials*, *2*(1), Article Number: 013605.

Smith, E.M., et al. (2016). Large gem diamonds from metallic liquid in Earth's deep mantle. *Science*, *354* (6318), 1403–1405.

Smith, E. M., et al. (2018b). Blue boron-bearing diamonds from Earth's lower mantle. *Nature*, *560*(7716), 84–85.

Smith, E. M., & Wang, W. (2016). Fluid CH4 and H2 trapped around metallic inclusions in HPHT synthetic diamond. *Diamond and Related Materials*, *68*, 10–12.

Sobolev, N. V., et al. (1997). Mineral inclusions in diamonds from the Sputnik kimberlite pipe, Yakutia. *Lithos*, *39*(3–4), 135–157.

Stachel, T., et al. (2000). Kankan diamonds (Guinea) II: Lower mantle inclusion parageneses. *Contribution to Mineralogy and Petrology*, *140*(1), 16–27.

Stachel, T., & Luth R. W. (2015). Diamond formation: Where, when and how? *Lithos*, *220–223*, 200–220.

Stoffler, D., et al. (1991). Shock metamorphism of ordinary chondrites. *Geochimica et Cosmochimica Acta*, *55*(12), 3845–3867.

Takafuji, N., et al. (2006). Decarbonation reaction of magnesite in subducting slabs at the lower mantle. *Physics and Chemistry of Minerals*, *33*(10), 651–654.

Taylor, W. R., Jaques, A. L., & Ridd, M. (1990). Nitrogen-defect aggregation characteristics of some Australasian diamonds: Time-temperature constraints on the source regions of pipe and alluvial diamonds. *American Mineralogist*, *75*, 1290–1310.

Thomson, A. R., et al. (2016). Slab melting as a barrier to deep carbon subduction. *Nature*, *529*(7584), 76–78.

Tschauner, O., et al. (2001). New transformations of CO2 at high pressures and temperatures. *Physical Review Letters*, *87*(7), Article Number: 075701.

Tschauner, O., et al. (2018). Ice-VII inclusions in diamonds: Evidence for aqueous fluid in Earth's deep mantle. *Science*, *359*(6380), 1136–1138.

van Keken, P. E., et al. (2002). Mantle mixing: The generation, preservation, and destruction of chemical heterogeneity. *Annual Review of Earth and Planetary Sciences*, *30*, 493–525.

von John, W. (1910). Native tantalum. *Nature*, *83*, 398.

Walter, M. J., et al. (2011). Deep mantle cycling of oceanic crust: Evidence from diamonds and their mineral inclusions. *Science*, *334*(6052), 54–57.

Yin, Z., et al. (2017). Inclusions of alpha-quartz, albite and olivine in a mantle diamond. *Gondwana Research*, *44*, 228–235.